



## Evaluation of adsorptive capacity of natural biosorbent for dye removal as a contribution to environmental protection: effect of various parameters

F. Ayari\*, S. Mezghuich, A. Ben Othmen, M. Trabelsi-Ayadi

*Laboratoire des Applications de la Chimie aux Ressources et Substances Naturelles et à l'Environnement (LACReSNE), Université de Carthage, Faculté de Sciences de Bizerte, Zarzouna 7021, Tunisia, Tel. +21621791747, email: fadhilaayari@yahoo.fr (F. Ayari), soumaya.mezguich@gmail.com (S. Mezghuich), benothman\_amel@yahoo.fr (A. Ben Othmen), malika.trabelsiayadi@gmail.com (M. Trabelsi-Ayadi)*

Received 26 November 2015; Accepted 17 February 2018

### ABSTRACT

In this study, natural bentonite was prepared and tested for the removal of diazo dye through the adsorption process. Investigated biosorbent was characterized using XRD, N<sub>2</sub> sorption, XRF, total surface area using methylene blue method and TEM techniques. The effect of major parameters, such as initial dye concentration, adsorbent dosage, pH, contact time and temperature were investigated and discussed. Results show that studied bentonite after purification exhibited high adsorption capacity toward acid dyes. Maximum adsorption of Congo red dye (CR) was achieved between pH 4 and 5. Kinetic study revealed that the adsorption profile is well fitted by the pseudo-second-order kinetic model and chemisorption process was proposed. Isotherm data were investigated according to Langmuir and Freundlich equations. Thermodynamic study showed the spontaneous nature of adsorption with endothermic process. Removal of lead heavy metal was investigated by adsorption into Congo red loaded purified bentonite and results show a high % removal (98.83 %).

*Keywords:* Bentonite; Adsorption; Acid textile dye; Sorption isotherms; Sorption kinetics; Langmuir and Freundlich models

### 1. Introduction

Textile industry generates large quantities of dye wastewater effluents. The discharge of these pollutants into natural water bodies raises environmental problems due to the pollution caused by their coloration [1]. It is a real degradation of the environment. Also has and an enormous harmful effect on the human health [2,3]. Especially, textile dyes present a very weak biodegradability [4] which makes the biological treatments difficult and in case of degradation, they may produce carcinogenic substances.

A study effected on chemical classifications of dyes, shows that diazo dyes are the most toxic [5]. Toxicity by exposure to azo dyes and their metabolites is not a new fact. Since 1895, the increase in the number of cancers of bladder observed in workmen of textile industry is connected to their exposure prolonged to the azo dyes [6].

Hence, alternative and efficient technologies for the removal of textile dyes are required. Several analytical processes have been used to remove dyes into wastewater such as chemical oxidation [7], coagulation [8], biological treatment [9], reverse osmosis [10], adsorption [11]. Among these processes, adsorption have attracted increasing interest because they could completely remove highly refractory organic pollutants such as azo dyes [12], heavy metals [13] and pharmaceutical compounds [14]. Among which, adsorption on activated carbon is an effective processes but it is expensive and produces a mud which constitutes itself an environmental threat [15]. To overcome these drawbacks, researchers increase interest into cheaper and more readily available adsorbents such as natural materials.

In recent years, attention has been focalized in clay mineral due to its abundance and availability, also according to its important surface and cation exchange capacity [16].

\*Corresponding author.

Previous studies have used clay mineral as adsorbent such as bentonite [17], sepiolite [18] and kaolinite [19] to remove dyes from wastewater.

However, several works were based on modification of these adsorbents via physical and chemical process [16], which is necessary for the adsorption of anionic dyes, as the net negative charge on the dye and clay surface brings charge repulsion and thus, resulting in lowering surface interaction and adsorption rate.

In this investigation, regarding their abundance and low-cost a locally Tunisian bentonite, without any further modification, was used to remove an anionic diazodye CR, very used in textile industry. The effect of different parameters such as pH, initial concentration of CR, adsorbent dose and temperature were studied to determine the best conditions of dye adsorption. Also, kinetics adsorption and thermodynamic studies were investigated.

## 2. Experimental section

### 2.1. Chemicals

Congo Red (CR) is a synthetic anionic secondary diazo dye (IUPAC name: [1-naphthalene sulfonic acid, 3,3-(4,4-biphenylenebis (azo))bis(4-amino-)disodium salt]) and used without any further purification in this study. The molecular weight is 696.66 g·mol<sup>-1</sup>, the maximum wavelength of CR in neutral medium is at  $\lambda_{\max} = 498$  nm and the structural formula is: C<sub>32</sub>H<sub>22</sub>N<sub>6</sub>Na<sub>2</sub>O<sub>6</sub>S<sub>2</sub>.

Molecular structure of this dye is represented in Fig. 1. As can be shown, it contains –NH<sub>2</sub> and –SO<sub>3</sub> functional groups. The CR sodium salts was the first synthetic dye capable of directly dyeing cotton [20]. It has a strong affinity for cellulose fibers and very used in textile industry.

The color of CR changes from red to blue in acidic medium. This change is due to the resonance between charged canonical structures [21] and the red color is stable in the pH range of 5–10 [22]. The stock solution of CR was prepared by dissolving known quantity of CR powder in distilled water and successive dilutions were made to obtain the working solution at desired concentrations.

### 2.2. Adsorbent preparation

Clay, used in this study, is a natural calcium smectite from a soil of Kef Abbed (north of Tunisia). This materials was previously crushed and sieved to reduce a particle size. Then, it underwent a purification stage as follows: a 100 g of raw clay was suspended in polyethylene bottle containing a solution of NaCl (1 M). After 12 h of agitation,

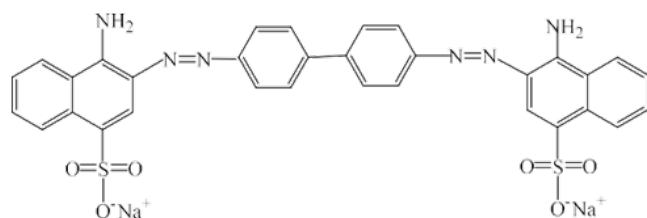


Fig. 1. Chemical structure of Congo red.

clay particles are separated from the solution by centrifugation at a speed of 6000 rpm for 30 min. This step is repeated several times to provide a complete substitution of the interlayer ions (Ca<sup>2+</sup>, Mg<sup>2+</sup>, Li<sup>+</sup>...) by sodium ion and finally obtain purified Na saturated clay. Impurities such as carbonate, quartz, calcite associated to the clay fraction were also eliminated.

The Na saturated clay is finally washed with distilled water several times; this step was followed by a dialysis process to remove the excess of chloride ions, AgNO<sub>3</sub> test is needed to verify the elimination of chloride ions. Obtained clay is dried at 333 K and then crushed and sieved.

The raw and purified bentonite being labeled ArB and ArP respectively.

### 2.3. Characterization methods

Composition of the clay sample was identified by X-ray diffractometer (XRD) and analysis was carried out using a PANalytical X'Pert High Score Plus diffractometer, CuK $\alpha$  radiation. Chemical composition of both samples was investigated by X-ray fluorescence spectrometer. Also, the composition of ArP sample was confirmed with EDX system. The Fourier transform infrared (FTIR) spectra were acquired on a Perkin Elmer 783 dispersive spectrometer in the range of 4000–400 cm<sup>-1</sup>. Cation exchange capacity (CEC) was estimated as described in previous studies [23,24]. Sample morphology was given by Transmission electron microscopy (TEM). BET surface area ( $S_{\text{BET}}$ ) and pore volumes of adsorbent were measured using the physical adsorption of nitrogen by Quantachrome Autosorb-1 instrument. The adsorption of methylene blue dye on bentonite in solution is used to determine either their cation-exchange capacities (CEC) or their total specific surface area (Ss) via UV-Vis spectrophotometer.

### 2.4. Adsorption experiments

The adsorption kinetics was carried out in a batch process. For each experiment, 50 ml of the CR solution at specified concentration were stirred with an amount of adsorbent during different time intervals (20–120 min). The suspensions were then centrifuged and the remained dye concentrations in the supernatant were measured with UV-visible spectrophotometer (Shimadzu Model Perkin Elmer) at 498 nm wavelength ( $\lambda_{\max}$ ).

The percentage adsorption of CR and equilibrium adsorption capacity,  $Q_e$  (mg/g), was calculated by the following relationships, respectively:

$$\% \text{ Adsorption} = 100 \frac{C_0 - C_e}{C_0} \quad (1)$$

$$q_e = V \frac{C_0 - C_e}{m} \quad (2)$$

where  $C_0$  and  $C_e$  are the initial and the equilibrium concentration of CR (mg·L<sup>-1</sup>), respectively.  $V$  is the volume of the dye solution, and  $m$  is the mass of adsorbent.

In this work, all adsorptions experiments were carried by the same way under several conditions such as pH, temperature, dye concentration and adsorbent dose.

### 3. Results and discussions

#### 3.1. Characterization of the adsorbent

##### 3.1.1. Chemical analysis

Chemical composition of raw and purified bentonite was performed by X-ray fluorescence spectrometer. Results are given in weight percent of oxides (Table 1).

A scan can be seen from Table 1, the presence of silica and alumina as major constituents with traces of potassium, magnesium and calcium oxides was confirmed [25].

From this analysis, the structural formula of the Na exchanged clay was investigated:

$\text{Ca}_{0.05} \text{Na}_{0.145} \text{K}_{0.479} (\text{Si}_{7.87} \text{Al}_{10.13}) (\text{Al}_{2.6} \text{Fe}_{0.678} \text{Mg}_{0.547}) \text{O}_{22}$ . This formula shows that the two types of substitutions exist (octahedral and tetrahedral substitutions) which gives a beidellitic-montmorillonitic character to this smectite.

##### 3.1.2. X-Ray diffraction

The clay sample, before and after purification, was analyzed by XRD measurements (Figs. 2 and 3). Results show that mineralogical composition of clay is composed mainly of smectite, kaolinite, illite, and quartz. The smectite is deduced by the existence of peaks at 15.3 Å on the raw sample which was shifted to 12.38 Å after purification and to 17.69 Å after ethylene glycol treatment. The presence of kaolinite was confirmed by the existence of peaks at 7.19 and 3.57 Å on the normal and glycoled diffractograms. These peaks disappear after calcinations at 550°C during 2 h. The appearance of peaks at 4.27 and 3.35 Å marked the presence of quartz, which disappears after purification, and peaks at 10.32 and 2.57 Å marked the presence of illite [26,27]. Heating the sample above 550°C collapses the interlayer spacing at 10 Å, this data support the clays smectite group.

##### 3.1.3. FTIR analysis

The FTIR spectra of purified and raw samples are shown in Fig. 4. The broad band's at around 3419 cm<sup>-1</sup> (H-O-H

stretching) and 1646 cm<sup>-1</sup> (H-O-H bending) indicate the presence of adsorbed water. The presence of an asymmetric stretching mode of Si-O-Si was suggested by the absorption bands at the range of 1035–1123 cm<sup>-1</sup>. The asymmetric and symmetric bending modes of O-Si-O are observed at 536 and 469cm<sup>-1</sup>, as in other silica and silicate systems.

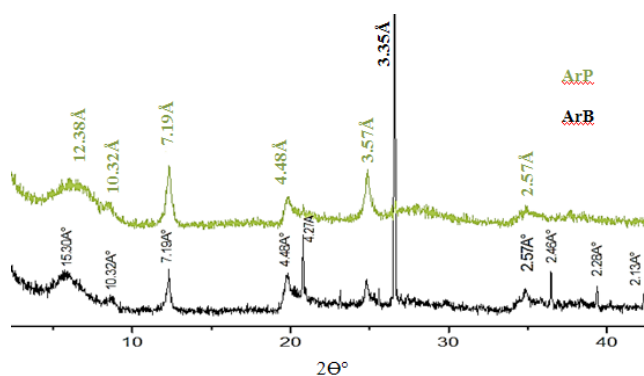


Fig. 2. X-ray diffractogram of ArB and ArP.

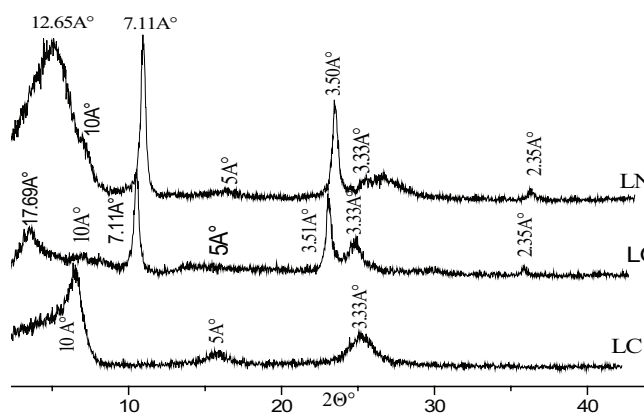


Fig. 3. Diffractogram of oriented samples of ArP (LC: heated blade, LG glycol blade; LN: normal blade).

Table 1  
Chemical composition (% weight (w %)) of raw and Sodium bentonite

$\text{M}_x\text{O}_y$ (w%) Sample	ArB	ArP
$\text{SiO}_2$	40.66	52
$\text{MgO}$	3.53	4.2
$\text{CaO}$	19	0.4
$\text{Fe}_2\text{O}_3$	4.89	4.8
$\text{Al}_2\text{O}_3$	9.23	15.3
$\text{Na}_2\text{O}$	1.16	1.63
$\text{K}_2\text{O}$	0.43	0.76

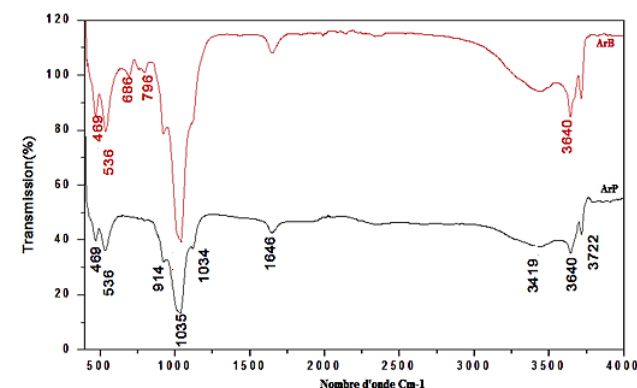


Fig. 4. Infrared spectrum of ArB and ArP.

The additional peaks at 686 and 796  $\text{cm}^{-1}$  in raw clay, which are absent in Na-bentonite, indicate the presence of quartz accompanying the crud sample, eliminated after purification [25].

### 3.1.4. Cation exchange capacity (CEC)

The cationic exchange capacity (CEC) was estimated using the copper ethylenediamine ((EDA)<sub>2</sub>CuCl<sub>2</sub>) complex [24]: it was calculated from the quantity of  $\text{Cu}(\text{EDA})_2^{2+}$  adsorbed by the clay. Results show that CEC value of clays samples decrease from 56.7 meq/100 g (ArB) to 98.87 meq/100 g (ArP), suggest that the clay sample used belonged to smectite group.

### 3.1.5. Specific surface area and porosity

#### 3.1.5.1. Total specific surface area Ss

Methylene blue dye (BM) adsorption on bentonite is used to determine either their cation exchange capacities (CEC) or their total specific surface area (Ss) [25]. In a series of 100 ml glass bottles, 20 ml of sorbent dosage ( $2\text{g}\cdot\text{L}^{-1}$ ) and a variable volume of methylene blue at initial concentration of  $0.5\text{g}\cdot\text{L}^{-1}$  were placed in consecutive order. The mixtures were kept at room temperature during 1 h under stirring. After centrifugation, the supernatant was analyzed by spectrophotometer at  $\lambda_{\text{max}} = 665\text{nm}$  (Fig. 5). Then, the amounts of each adsorbed solution were determined and these val-

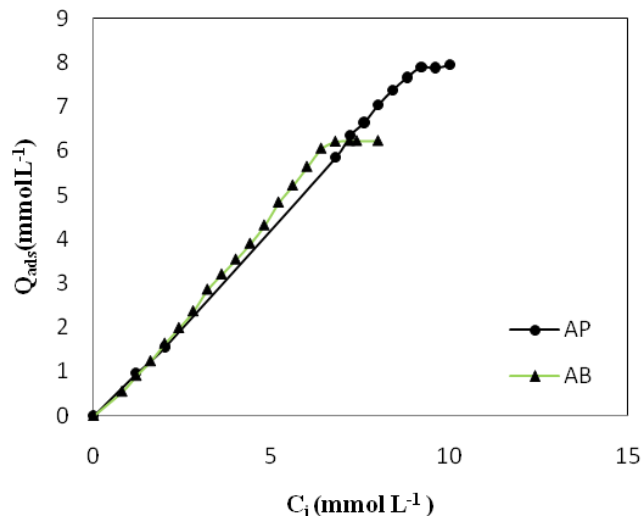


Fig. 5. Uptake of MB by clay sample before (ArB) and after purification (ArP) to estimate CEC and Ss of the clay sample  $Q_{\text{ads}}$ : Amount of MB adsorbed by clay sample.  $C_i$ : initial concentration of MB.

Table 2  
Specific surface area and CEC (methylene blue method)

	Ss ( $\text{m}^2\cdot\text{g}^{-1}$ )	CEC (meq/100 g)
ArP	902	97.83
ArB	492	62.3

ues allowed the determination of both CEC and Ss (Table 2). The highest values of Ss and CEC indicate that this clay belongs to bentonite type. It can be noticed that the CEC values of ArP and ArB agree well with those determined by copper ethylenediamine method.

#### 3.1.5.2. Adsorption $\text{N}_2$

Fig. 6 shows the  $\text{N}_2$  isotherms at 77 K for raw and purified clays. The isotherms are of type IV, corresponding tomicroporous solids. Both samples show a hysteresis loop type H4 according to IUPAC classification.

Table 3 presents the values for specific surface area,  $S_{\text{BET}}$ , volume of  $\text{N}_2$  adsorbed at  $P/P_0 = 0.98$ ;  $V_{\text{ads}}$ , mesoporosity surface and volume;  $S_{\text{BJH/mes}}$  and  $V_{\text{BJH/mes}}$  respectively, from the Barret-Joyner-Halenda method and average

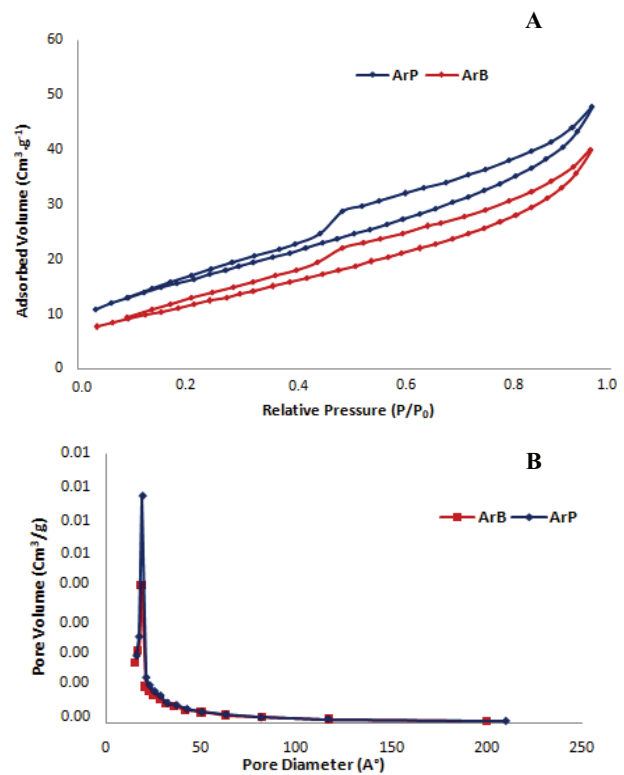


Fig. 6. Nitrogen adsorption/desorption isotherms at 77 K for raw and purified bentonite (A). And BJH-method pore size distribution curves from nitrogen sorption data (B).

Table 3  
Textural properties of both samples

Sample	ArB	ArP
$S_{\text{BET}}$ ( $\text{m}^2/\text{g}$ )	42.695	57.963
$V_{\text{tot}}$ (cc/g)	0.06	0.07
D ( $\text{Å}$ )	19.003	19.109
$S_{\text{BJH}}$ ( $\text{m}^2/\text{g}$ )	31.051	38.316
$V_{\text{mes}}$ (cc/g)	0.051	0.059

pore diameter ( $D$ ) of both samples. It can be seen that  $S_{\text{BET}}$  increase after purification which confirm that purification stage took place.

### 3.2. Adsorption studies

#### 3.2.1. Kinetic study

The adsorption data of CR uptake onto ArP and ArB versus contact time are presented in Fig. 7. According to this figure, adsorption kinetics of CR by ArP and ArB takes the same forms characterized by a strong increase of the adsorption in the first minutes of contact time (adsorbate-adsorbent), followed by a slow increase until reaching equilibrium which is less than 40 min. The highest percent of CR removal was attributed to ArB sample (Fig. 7). This can be explained by the fact that in the interlayer sheet of the raw sample there is bivalent ( $\text{Ca}^{2+}$ ,  $\text{Mg}^{2+}$ ...) and monovalent ( $\text{Na}^+$ ,  $\text{K}^+$ ,  $\text{Li}^+$ ...) cations, so much more positive charges exist in the raw sample, contrary to ArP which was saturated, after purification, only with monovalent cations ( $\text{Na}^+$ ). However, ArP has been used as adsorbent for the rest of adsorption experiments because of its interlayer homogeneity which can simplify the comprehension of adsorption mechanism.

From the literature, adsorption of a solute by a solid in aqueous solution is a phenomenon whose kinetics are often complex. The adsorption rate is strongly influenced by several parameters related to the state of the solid, generally having very heterogeneous reactive surface and to the physicochemical conditions under which adsorption is carried out.

In order to analyze experimental data, it is necessary to identify the step that governs the overall removal rate in the adsorption process. In general, adsorption may be described as a series of steps [28]: (i) Transport of the adsorbate from the fluid to the external adsorbent surface through the boundary layer (film diffusion), (ii) diffusion of the adsorbate within the pores of the adsorbent (particle diffusion), (iii) Adsorption itself onto the surface.

Certain kinetic models are available to understand the behavior of the adsorbent and to predict the mechanism involved in the sorption process. Pseudo-first-order and pseudo-second-order models are the most frequently used in the literature [29].

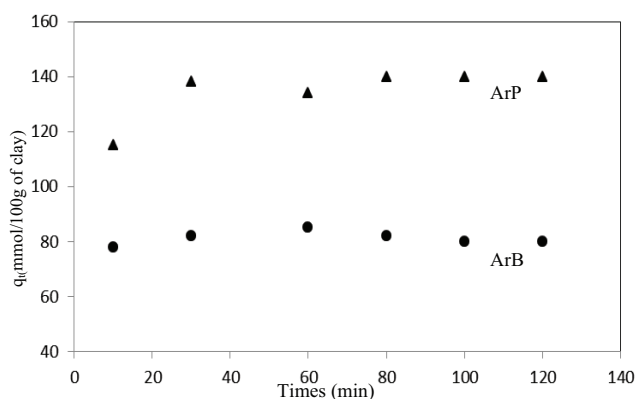


Fig. 7. Kinetic of CR adsorption in ArB and ArP.

#### 3.2.1.1. Pseudo-first-order kinetics models

The pseudo-first-order model can be expressed by the following equation [29,30]:

$$\frac{dq}{dt} = K_1(q_e - q_t) \quad (3)$$

After the integration at initial condition  $q_t = 0$  at  $t = 0$ ; Eq. (4) can be given:

$$\ln(q_e - q_t) = \ln q_e - k_1 t \quad (4)$$

where  $q_e$  and  $q_t$  ( $\text{mg}\cdot\text{g}^{-1}$ ) are the adsorption capacity at equilibrium and at time  $t$ , respectively;  $K_1$  ( $\text{min}^{-1}$ ) is the rate constant of the pseudo-first adsorption. The validity of this model can be squared by linearized plot of  $\ln(q_e - q_t)$  versus time ( $t$ ) (Fig. 8a). The rate constant  $K_1$  and the correlation coefficients were estimated from the slope of the plot and illustrated in Table 4. The calculated equilibrium adsorption capacity  $q_{e(\text{cal})}$  seemed to be much lower than the experimental values  $q_{e(\text{exp})}$ . Also, correlation coefficients of the pseudo first-order model ( $R^2 = 0.605$ ) are low. According to these results, it can be concluded that the pseudo-first order kinetic don't fit very well the experimental data.

#### 3.2.1.2. Pseudo-second-order kinetics models

The pseudo second-order kinetic equation based on the adsorption capacity is given by Eq. (5) [29,30]:

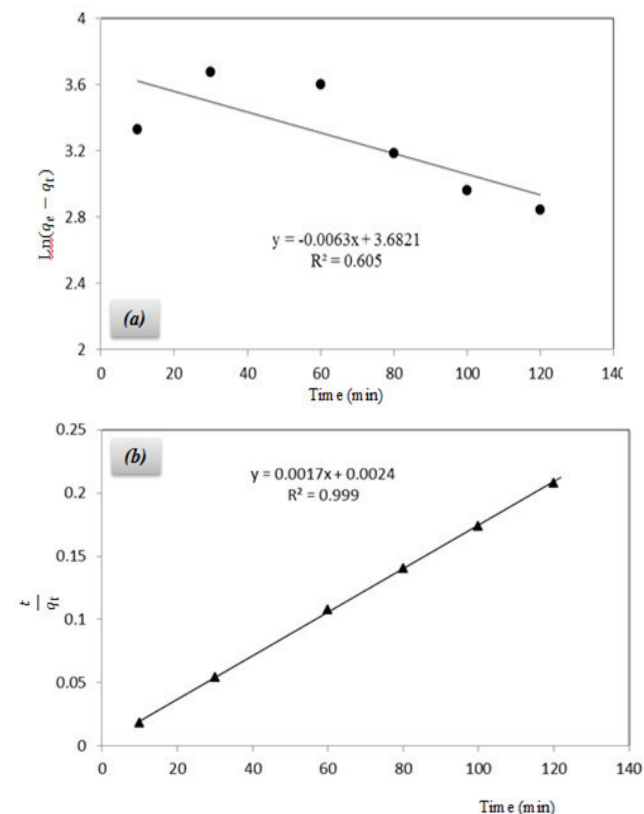


Fig. 8. The first order (a) and the second order (b) Pseudo kinetics for adsorption of CR by ArP.

Table 4  
Kinetic parameters of the pseudo first and second order

Pseudo first order			Pseudo second order			$q_{e(exp)}$
$K_1$	$q_{e(cal)}$	$R^2$	$K_2$	$q_{e(cal)}$	$R^2$	
0.0063	39.720	0.605	0.0012	588.230	0.999	585.194

$$\frac{dq}{dt} = K_2 (q_e - q_t)^2 \tag{5}$$

Considering the initial condition, integration of Eq. (6) gives:

$$\frac{t}{q_t} = \frac{1}{k_2 q_e^2} + \frac{t}{q_e} \tag{6}$$

where  $q_e$  and  $q_t$  ( $mg \cdot g^{-1}$ ) are the adsorption capacity at equilibrium and at time  $t$ , respectively;  $K_2$  ( $g \cdot mg^{-1} \cdot min^{-1}$ ) is the rate constant of the pseudo-second-order adsorption. This model can be squared by a linearized plot  $t/q_t$  of versus time ( $t$ ) (Fig. 8-b). The rate constant  $K_2$  and  $q_e$  are determined from the intercept and slope of the plot (Table 4). It can be seen that the maximum adsorption capacity,  $q_{e(cal)}$ , is in accordance with the experimental values. In addition, a high correlation coefficient  $R^2$  was obtained ( $R^2 = 0.999$ ). These finding suggest that Congo red dye adsorption obeys a pseudo-second-order model and the confirmation of the assumption [31] that the rate limiting-step of Congo red onto ArP may be chemisorption which involves valence forces by sharing or electron exchange between the adsorbent and the adsorbate [32]. Chen et al. [16] report the same results for the adsorption of Congo red dye onto organo-attapulgit showing that pseudo-second-order is the most reliable model and the chemisorption in the main rate controlling step of the adsorption process.

Similar results for the adsorption of acid dyes have also been reported by other researchers [33–35].

### 3.2.2. Sorption isotherms

Adsorption isotherms were determined at 25°C by shaking 100 mg of the adsorbent (ArP) with 50 ml of CR solution with variant concentrations for 60 min. After shaking at 5000  $tr \cdot min^{-1}$ , the solution was separated from the solid by centrifugation. The residual concentrations in the supernatants were determined by UV-Visible spectrophotometer at 498 nm, and the solid phases were analyzed by FTIR spectroscopy at the range of 400–4000  $nm^{-1}$ .

According to Giles classification [36], adsorption isotherms of congo red by ArP (Fig. 9), expressing the adsorbed amounts ( $q_e$ ) as a function of equilibrium concentration ( $C_e$ ), seem to be of the L-type. In this kind of isotherm, the initial portion provides information about the availability of the active sites to the adsorbate and the plateau suggests a monolayer formation. The initial curvature indicates that a large amount of dye is adsorbed at a lower concentration as more active sites of ArP are available. As the concentration increases, it becomes difficult for a dye molecules to find vacant sites, and so monolayer formation occurs.

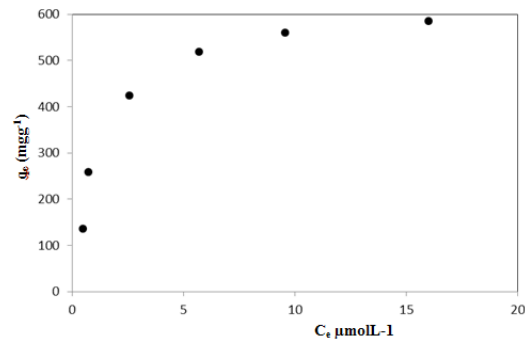


Fig. 9. Adsorption isotherm of CR by ArP.

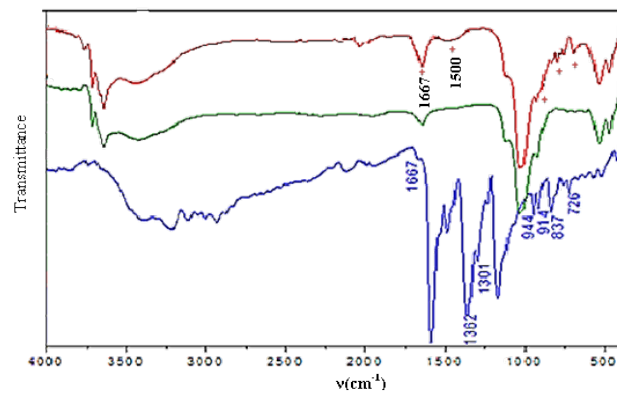


Fig. 10. FTIR spectrums of: (a) CR powder only, (b) ArP before CR adsorption and (c) ArP after CR adsorption.

Table 5  
Most important adsorption bands of CR functional groups

Functional groups	Frequency ( $cm^{-1}$ )
$u(C=C)_{Ar}$	1667
$u(N-H)$	1500
$d(C-H)_{Ar}$	837-914 -726

Uptake of CR by ArP has been confirmed by FTIR study (Fig. 10). Results show new absorption bands in ArP FTIR spectrum after dye adsorption, in comparison with FTIR spectrums of ArP and CR, these bands linked to specific functionals groups of CR structure (Table 5).

### 3.2.3. Effect of pH on dye removal

Dye adsorption onto clay is strongly dependent on pH solution [37]. This can be attributed to the chemical form of dye in solution and functional groups present on the adsorbent surface at a specific pH [38]. CR is a diazo anionic dye and is a pH sensitive, exposure to HCl causes color change from red to blue (Fig. 11), due to  $\pi-\pi^*$  transition of azo group shift to higher wavelength because of protonation [39]. At lower pH, CR become cationic and shows two tautomeric

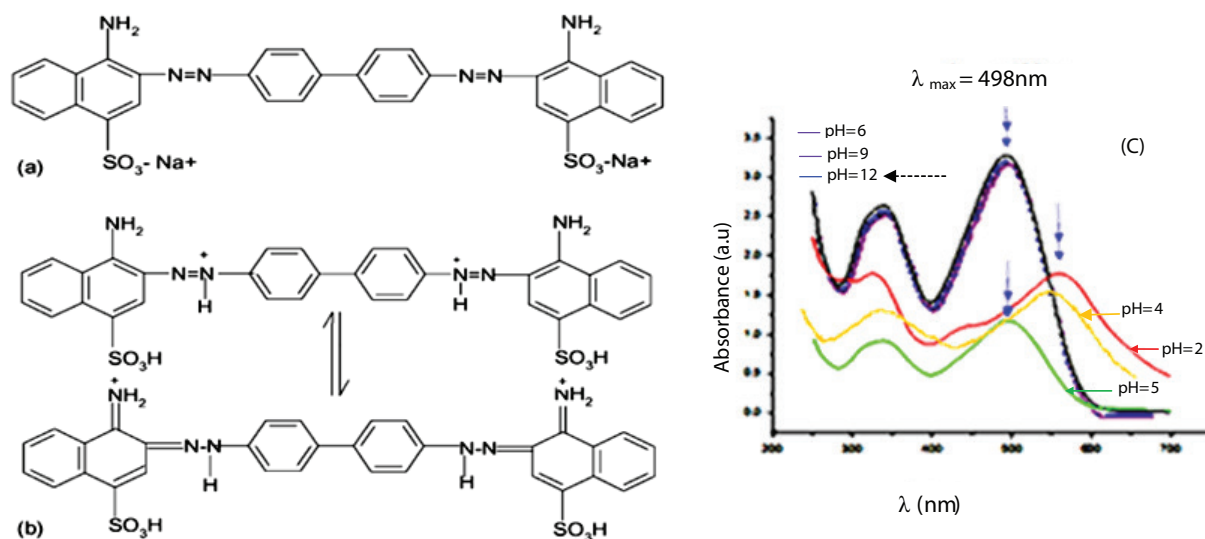


Fig. 11. Structure of Congo red at (a) pH > 5.5, (b) pH < 5.5 [39,40], (c) Experimental values of  $\lambda_{\max}$ .

forms of protonated CR [40], i.e. ammonium rich variety and azonium variety (Fig. 11b).

In this work, effect of initial pH on the amount of adsorbed dye was studied at 25°C over a range of pH from 2 to 12. Experiments were conducted on suspensions of 0.1g of ArP in 50 ml of dye solution with initial concentration of 69.66 mg·L<sup>-1</sup>. The suspensions were stirred for 1 h and then centrifuged. Dye concentrations in the supernatant were measured by UV-visible spectrophotometer at the specific  $\lambda_{\max}$  which is determined experimentally (Fig. 11c). The pH was adjusted by adding a few drops of NaOH (0.1 M) or HCl (0.1 M) before each experiment.

As shown in Fig. 12, the amount of dye adsorbed per unit mass of adsorbent at equilibrium increased as pH was increased from 2 to 5, reaching a maximum at pH range 4–5 with 92% of dye removal. We have noted an almost complete discoloration of the solution for pH range 4–5. The maximum adsorption can be estimated at pH = 4.5.

At lower pH, the negatively charged silica sites of bentonite are neutralized by H<sup>+</sup> ions and alumina sites are positive, the number of negatively surface charged decrease. However, significant CR adsorption was reached. On the other hand, at lower pH CR (dipolar molecule H<sub>3</sub>N<sup>+</sup>-R-SO<sub>3</sub><sup>-</sup>) presents two protonated tautomeric species (Fig. 11b): an ammonium form, where the protons attached to the amino nitrogen and an azonium form, they were attached to the  $\alpha$ -azo nitrogen. Many functional N-sites are presented on CR and some of nitrogen form hydrogen bonds by accepting protons from the solution and some are protonated to form cationic species.

Therefore, the maximum adsorption of cationic dye at lower pH may be due to the mechanism of cation exchange, replacing Na<sup>+</sup>, initially present in the interlayer space of bentonite. Thereafter, adsorption decreased with increasing pH. Above pH 6, the percentage of dye removal drops. The overhead setup can be attributed to the changes in the polarity of the electric double layer on both the silica and alumina contents of the clay from positive to negative. The high negatively charged adsorbent surface sites (at high pH) did not favor the adsorption of deprotonated CR due

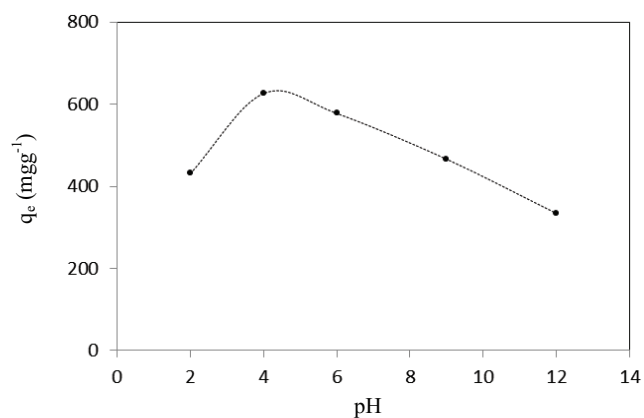


Fig. 12. Effect of pH on CR removal by ArP.

to electrostatic repulsion. Also, an abundance of OH<sup>-</sup> ions in basic solution creates a competitive environment with anionic ions of CR for the adsorption sites causing a significant reduction in the removal of CR dye from the solution.

Previous works [41] suggest that -NH<sub>2</sub>, -N=N-, -HN-N and SO<sub>3</sub><sup>-</sup> groups of CR were involved in the adsorption. Adsorption of CR by ArP has been confirmed by the appearance of some of this functional group in IR spectrum of clay sample after dye adsorption (Fig. 10).

### 3.2.4. Effect of adsorbent dosage

The effect of ArP adsorbent dosage on the removal of CR anionic dye (at natural pH) is illustrated in Fig. 13. It can be seen that the percentage of CR removal increased with the increase in adsorbent dosage. This can be attributed to the increase of adsorbent surface area and availability of more adsorption active sites resulting from the increase dosage of the adsorbent. Previous studies showed a similar behavior for other dyes, for example, Ashraf et al. [42] reported that acid yellow sorption onto biosorbent 'Typhaangustata'

increased with the increase of adsorbent dose, which was due to the formation of a large number of adsorbing sites.

### 3.2.5. Influence of temperature

Effect of temperature on CR dye removal was investigated at 20, 30, 40 and 50°C (Fig. 14). It could be clearly seen that, the amount adsorbed at equilibrium increases with increasing temperature. When the temperature increased from 20°C to 50°C, the maximum amounts of CR removed by this purified bentonite (ArP) are found to be increased from 581 to 638.837 mg.g<sup>-1</sup>, estimated a complete removal of this dye by clay mineral without any further modification. Therefore, this system was endothermic which is more favorable at higher temperature.

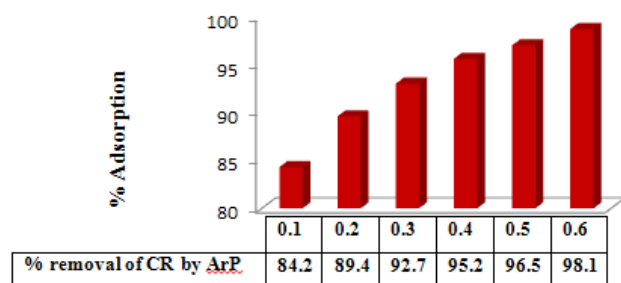


Fig. 13. Effect of adsorbent (ArP) dose on the removal of CR.

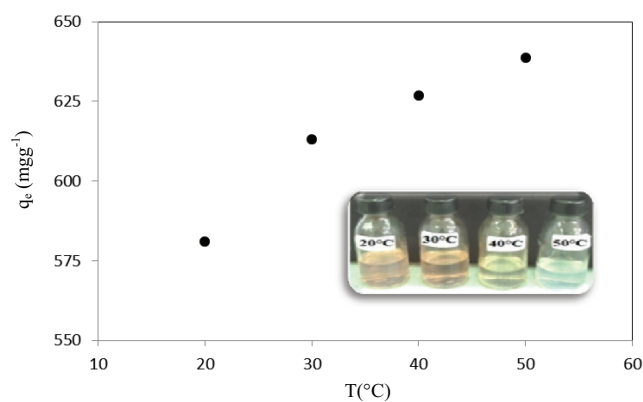


Fig. 14. Effect of temperature on CR removal.

It is found that higher temperature enhances the sorption of CR. It is common that increasing temperature may cause a swelling influence in the adsorbent structure leading to the insertion of supplementary dye molecules. But, it is necessary to note that in some previous studies [43,44] an increase in temperature may cause an increase or a decrease in the amount of dye adsorbed by various kinds of clay minerals.

### 3.3. Modelization of experimental data

Equilibrium data of Congo red adsorption onto purified bentonite (ArP) were analyzed using the linearized form of Freundlich and Langmuir models.

#### 3.3.1. Langmuir model

The Langmuir model [45] assumes monolayer adsorption on a uniform surface with a finite number of adsorption sites. Once a site is occupied, no further sorption can take place at that site, the surface will eventually reach a saturation point where the maximum adsorption of the surface will be achieved. The linear form of the Langmuir isotherm model [Eq. (7)] is given in Table 6.

Accordingly, experimental adsorption data were analyzed using the linearized form of Langmuir isotherm, obtained by plotting  $C_e/q_e$  versus  $C_e$  (Fig. 15). The calculated Langmuir isotherm constants and the corresponding coefficient of correlation,  $R^2$  are shown in Table 6.

#### 3.3.2. Freundlich model

The Freundlich adsorption is applicable to monolayer (chemisorption) and multilayer adsorption (physisorption) and is based on the assumption that the adsorbate adsorbs onto the heterogeneous surface of an adsorbent [46]. The linear form of Freundlich equation [Eq. (8)] is given in Table 6.

The equilibrium data were further analyzed using the linearized form of Freundlich isotherm, by plotting  $\ln q_e$  versus  $\ln C_e$  (Fig. 16). The calculated Freundlich isotherm constants ( $K_F, n$ ) and the corresponding coefficient of correlation,  $R^2$  are shown in Table 6.

As can be noted from modelization results, experimental data agree very well with Langmuir model ( $R^2 = 0.996$ ) compared to Freundlich equation ( $R^2 = 0.861$ ). Also, the value of maximum adsorption capacity,  $q_m$ , calculated from

Table 6  
Langmuir and Freundlich parameters

Langmuir model		Freundlich model			
Linearized equations		$\ln q_e = 1/n \ln C_e + \ln K_F$ (8)			
$\frac{C_e}{q_e} = \frac{1}{k_L q_m} + \frac{C_e}{q_m}$ (7)					
$q_m$ : maximum adsorption capacity (mg.g <sup>-1</sup> )	$K_L$ Langmuir constant (L.mg <sup>-1</sup> )	$C_e$ : equilibrium concentration (mg.L <sup>-1</sup> )	$n$ : adsorption intensity	$K_F$ : Freundlich constant (L.mg <sup>-1</sup> )	
$R^2$	$R_L$	$K_L$	$q_m$	$R^2$	$1/n$
0.996	0.014	1	1000	0.861	0.401
					$K_F$
					264.01

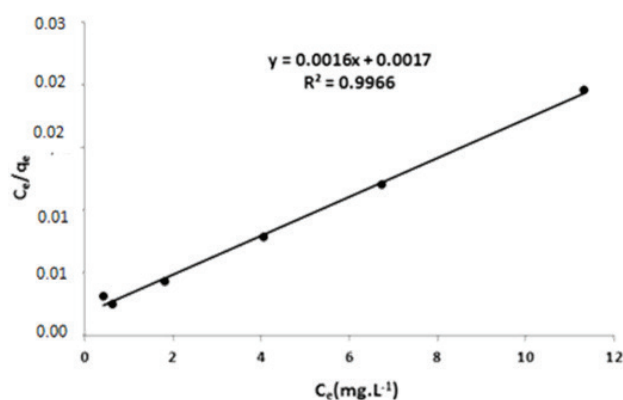


Fig. 15. Langmuir plots of CR by ArP.

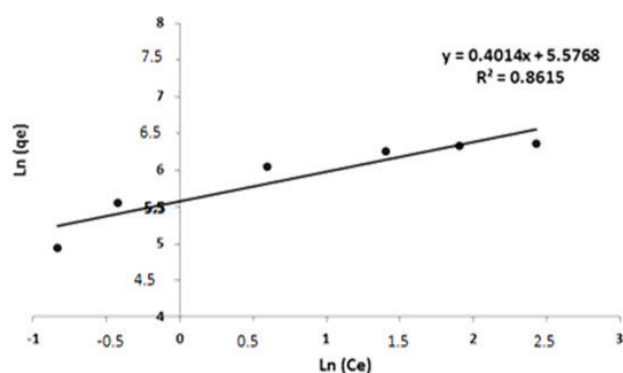


Fig. 16. Freundlich plots of CR by ArP.

Langmuir plot close the experimental value. Hence, it can be deduced that CR adsorption into ArP sample, without any further modification, is a monolayer adsorption mechanism with a good rate of removal.

The same results were reported for the CR adsorption onto coal-based mesoporous activated carbon [15], flyash [11] and organo-attapulgitic [16] confirming the monolayer adsorption.

Essential characteristics of Langmuir isotherm can be expressed in terms of a dimensionless constant assigned to as separation factor  $R_L$  that is given by the following equation:

$$R_L = \frac{1}{(1 + K_L C_0)} \quad (9)$$

where  $C_0$  ( $\text{mg}\cdot\text{L}^{-1}$ ) is the initial concentration of adsorbate, and  $K_L$  is Langmuir constant. The value of  $R_L$  indicates the shape of the isotherm which is [13]: (i) unfavorable ( $R_L > 1$ ), (ii) linear ( $R_L = 1$ ), (iii) favorable ( $0 < R_L < 1$ ), (iv) or irreversible ( $R_L = 0$ ). The  $R_L$  values are observed to be in the range 0–1 (Table 6), indicating that the adsorption was a favorable process.

### 3.4. Thermodynamics study

Adsorption process is always accompanied by a thermal process [47] which can be either exothermic ( $\Delta H <$

0) or endothermic ( $\Delta H > 0$ ). The measurement of  $\Delta H^0$  is a main parameter to understand the adsorption mechanism: chemisorption or physisorption. So, according to Gibbs-Helmholtz relationship [48] the heat of adsorption  $\Delta H^0$  is given as follows:

$$\Delta G = \Delta H - T\Delta S \quad (10)$$

where  $\Delta G^0$  Gibbs free energy ( $\text{KJ}\cdot\text{mol}^{-1}$ ),  $\Delta H^0$  enthalpy ( $\text{KJ}\cdot\text{mol}^{-1}$ ),  $\Delta S^0$  entropy ( $\text{KJ}\cdot\text{mol}^{-1}\cdot\text{K}^{-1}$ ) and  $T$  temperature (K).

The enthalpy  $\Delta H$  and entropy  $\Delta S$  were determined according to following equations (Eq. (11)) and (Eq. (12)):

$$\Delta G = -RT \ln Kc \quad (11)$$

$$\ln K = \left( \frac{\Delta S^0}{R} \right) - \left( \frac{\Delta H^0}{RT} \right) \quad (12)$$

where  $R$  is the universal gas constant ( $8.3143 \text{ J}\cdot\text{mol}^{-1}\cdot\text{K}^{-1}$ ) and  $K$  is the distribution coefficient, calculated as follows:

$$K = \frac{q_e}{C_e} \quad (13)$$

where  $q_e$  ( $\text{mg}\cdot\text{g}^{-1}$ ) is the equilibrium Congo red concentration adsorbed onto purified clay and  $C_e$  ( $\text{mg}\cdot\text{L}^{-1}$ ) is the equilibrium concentration of Congo red in solution.

Using the predict equations and plotting  $\ln K$  vs. temperature ( $T$ ) graphic (figure not shown), thermodynamics parameters were calculated and results are shown in Table 7. As can be seen, the positive values of  $\Delta H$  confirm the endothermic nature of adsorption process and its low values ( $< 40 \text{ KJ}\cdot\text{mol}^{-1}$ ) indicate that this is a physical adsorption [49]. The negative values of  $\Delta G^0$  represent the adsorption process of CR into ArP is favorable and spontaneous in nature. The positive values of  $\Delta S$  show the increased disorder at the solid solution interface components.

### 3.5. Application to remove lead heavy metal from wastewater

Wastewater contained heavy metals, considered as toxic and mutagenic elements [50]. So, in order to treat these environmental problems, the complexed Congo red-saturated Na bentonite ArP was used as adsorbent to remove lead heavy metal. For this experiment, the same conditions of CR adsorption were applied (natural pH, ambient temperature, 0.1 g of complexed CR-ArP). Aqueous solution of lead was prepared from  $\text{Pb}(\text{NO}_3)_2$  and the concentration is in order to the ArP clay CEC. ArP was also tested as adsorbent to remove lead heavy metal solution.

We reported that the final pH value of CR loaded ArP suspension is 6.5 and the initial pH value of the lead aqueous solution were fixed at pH 5. Results are shown in Table 8. It can be seen that the complex CR-ArP exhibited a high % adsorption of Pb reached 98.83 % compared with ArP which presents only 40.65%. This high % adsorption of lead by CR-ArP is due to electrostatic attraction between the positive charge of cationic heavy metal and the negative charge of sulfonate group ( $\text{SO}_3^-$ ) in Congo red loaded into purified clay (CR-ArP). According to our previous work [13,25], in the pH range between 6–7 a significant amount of  $\text{Pb}(\text{II})$  hydroxide  $\text{Pb}(\text{OH})^+$  may be present in the solution

Table 7  
Experimental results of thermodynamics of Congo Red adsorption

Temperature (K)	293	303	313	323
$\Delta G$ (KJ.mol <sup>-1</sup> )	-0.914	-1.865	-2.815	-3.765
$\Delta H$ (KJ.mol <sup>-1</sup> )	23.930			
$\Delta S$ (J.mol <sup>-1</sup> .K <sup>-1</sup> )	95.034			

Table 8  
Removal of Pb with different adsorbents

Adsorbents	% Adsorption
ArP	40.65
CR-ArP	98.83

and in this condition the adsorption process of Pb was supplemented by the retention of Pb(OH)<sup>+</sup>.

#### 4. Conclusion

In this investigation, Ca-bentonite was collected, purified and used without any further modification, as adsorbent for treatment of industrial wastewater and water polluted with anionic dyes. Adsorption results reveal the following conclusions:

- Amount of CR adsorbed was found to increase with the increase of initial CR concentration, adsorbent dosage, temperature and pH in the range of 4–5,
- Adsorption reached equilibrium inside 40 min,
- Experimental data fit very well with Langmuir isotherm model, which suggests a monolayer adsorption process,
- Adsorption kinetics followed a pseudo-second-order kinetic model. This indicates that chemisorption could be the adsorption mechanism of dye removal by Na saturated bentonite (ArP),
- Thermodynamic study confirms the endothermic nature of this process.

As contribution to valorization of waste from adsorption process, the complex CR loaded into ArP was tested in lead heavy metal removal and results show a high % removal compared to ArP only. This is due to electrostatic interaction between negative charges in sulfonate group (SO<sub>3</sub><sup>-</sup>) in CR and positive charges in Pb<sup>2+</sup> and Pb(OH)<sup>+</sup> species.

#### References

- [1] Y. Shengquan, W. Hui, Z. Chao, H. Fu, Separation of carcinogenic aromatic amines in the food colorants plant wastewater treatment, *Desalination*, 222 (2008) 294–301.
- [2] T. Robinson, G. McMullan, R. Marchant, P. Nigam, Remediation of dyes in textile effluent: a critical review on current treatment technologies with a proposed alternative, *Biores. Tech.*, 77 (2001) 247–255.
- [3] A.M.S. Solano, C.K.C. de Araújo, J.V. de Melo, J.M. Peralta-Hernández, D.R. da Silva, C.A. Martínez-Huitle, Decontamination of real textile industrial effluent by strong oxidant species electrogenerated on diamond electrode: Viability and disadvantages of this electrochemical technology, *Appl. Catal. B: Environ.*, 130 (2013) 112–120.
- [4] N. Kannan, M.M. Sundaram, Kinetics and mechanism of removal of methylene blue by adsorption on various carbons: a comparative study, *Dyes Pig.*, 51 (2001) 25–40.
- [5] H. Zollinger, *Color Chemistry-Synthesis, Properties of Organic Dyes* Fig. VCH Publishers, New York, 1987, pp. 92–100.
- [6] L. Rehn, BlasengeschulstebeiFuschin-arbeiten, *Arch. Klin. Chir.*, 50 (1895) 588–600.
- [7] M. Neamtu, A. Yediler, I. Siminiceanu, M. Macoveanu, A. Kellrup, Decolorization of disperse red 354 azo dye in water by several oxidation processes—a comparative study, *Dyes Pig.*, 60(1) (2004) 61–68.
- [8] P.J. Halliday, S. Beszedits, Color removal from textile mill wastewaters, *J. Can. Text.*, 103 (1986) 78–84.
- [9] S.S. Patil, V.M. Shinde, Biodegradation studies of aniline and nitrobenzene in aniline plant wastewater by gas chromatography, *Environ. Sci. Technol.*, 22(10) (1988) 1160–1165.
- [10] G.S. Gupta, G. Prasad, V.N. Singh, Removal of chrome dye from aqueous solutions by mixed adsorbents: Fly ash and coal, *Water Res.*, 24(1) (1990) 45–50.
- [11] V.V.B. Rao, S.R.M. Rao, Adsorption studies on treatment of textile dyeing industrial effluent by fly ash, *Chem. Eng. J.*, 116(1) (2006) 77–84.
- [12] C. Pelekani, V.L. Snoeyink, A kinetic and equilibrium study of competitive adsorption between atrazine and Congo red dye on activated carbon: the importance of pore size distribution, *Carbon*, 39(1) (2001) 25–37.
- [13] F. Ayari, E. Srasra, M. Trabelsi-Ayadi, Retention of lead from an aqueous solution by use of bentonite as adsorbent for reducing leaching from industrial effluents, *Desalination*, 206 (2007) 270–278.
- [14] E.M. Cuerda-Correa, J.R. Domínguez-Vargas, F.J. Olivares-Marín, J.B. deHeredia, On the use of carbon blacks as potential low cost adsorbents for the removal of non-steroidal anti-inflammatory drugs from river water, *J. Hazard. Mater.*, 177(1) (2010) 1046–1053.
- [15] E. Lorenc-Grabowska, G. Gryglewicz, Adsorption characteristics of Congo red on coal-based mesoporous activated carbon, *Dyes Pig.*, 74(1) (2007) 34–40.
- [16] H. Chen, J. Zhao, Adsorption study for removal of Congo red anionic dye using organo-attapulgit, *Adsorption*, 15 (2009) 381–389.
- [17] A. Berez, G. Schafer, F. Ayari, M. Trabelsi-Ayadi, Adsorptive removal of azo dyes from aqueous solutions by natural bentonite under static and dynamic flow conditions, *Int. J. Environ. Sci. Technol.*, 13(7) (2016) 1625–1640.
- [18] M. Alkan, S. Çelikçapa, S.Ö. Demirba, Removal of reactive blue 221 and acid blue 62 anionic dyes from aqueous solutions by sepiolite, *Dyes Pig.*, 65(3) (2005) 251–259.
- [19] R.G. Harris, J.D. Wells, B.B. Johnson, Selective adsorption of dyes and other organic molecules to kaolinite and oxide surfaces, *Colloids Surf. A: Physicochem. Eng. Aspects.*, 180(1–2) (2001) 131–140.
- [20] M.K. Purkait, A. Maiti, S. DasGupta, S. De, Removal of Congo red using activated carbon and its regeneration, *J. Hazard. Mater.*, 145 (2007) 289–295.
- [21] I.L. Finar, *Organic Chemistry The Fundamental Principles*, 1, sixth ed., Addison. Wesley Longman Ltd., England., 1986.
- [22] A.S. Özcan, A. Özcan, Adsorption of acid dyes from aqueous solutions onto acid-activated bentonite, *J. Colloid Interface Sci.*, 276 (2004) 39–46.
- [23] I. Mantin, Mesure de la capacité d'échange cationique des minéraux argileux par l'éthylène diamine et les ions complexes de l'éthylène diamine, *C.R. Sci. Paris.*, 269 (1969) 815–818.
- [24] F. Bergaya, M. Vayer, CEC of clay Measurement by adsorption of a copper éthylènediaminecomplexem, *Appl. Clay. Sci.*, 12 (1997) 275–280.

- [25] F. Ayari, E. Srasra, M. Trabelsi-Ayadi, Characterization of bentonitic clays and their use as adsorbent, *Desalination*, 185 (2005) 391–397.
- [26] I. Jarraya, S. Fourmentin, M. Benzina, S. Bouaziz, VOCs adsorption on raw and modified clay materials, *Chem. Geo.*, 275(1–2) (2010) 1–8.
- [27] M. Sakizci, B. Alver, E. Yorukogullari, Complex investigations of structural and thermal properties of silica-titania adsorbents, *J. Therm. Anal. Calorim.*, 98 (2009) 429–436.
- [28] D. David, R. Caplain, Méthodes usuelles de caractérisation des surfaces, Eyrolles, Paris (1988) 374 p.
- [29] Y.S. Ho, J.C.Y. Ng, G. McKay, Kinetics of pollutant sorption by biosorbents: Review, *Separ. Purif. Meth.*, 29 (2000) 189–232.
- [30] Y.S. Ho, G. McKay, Kinetic models for the sorption of dye from aqueous solution by wood, *Proc. Saf. Env. protec.*, 76 (1998) 183–191.
- [31] Y.S. Ho, G. McKay, Pseudo-second order model for sorption processes, *Process Biochem.*, 34(5) (1999) 451–465.
- [32] L. Wang, A. Wang, Adsorption properties of Congo Red from aqueous solution onto surfactant-modified montmorillonite, *J. Hazard. Mater.*, 160 (2008) 173–180.
- [33] A. Khenifi, Z. Boubberka, F. Kameche, Z. Derriche, Adsorption study of an industrial dye by an organic clay, *Adsorption*, 13 (2007) 149–158.
- [34] M.N. Chong, B. Jin, C.W.K. Chow, C. Saint, Recent developments in photocatalytic water treatment technology: a review, *Water Res.*, 44 (2010) 2997–3027.
- [35] M.A. Ashraf, M.A. Rehman, Y. Alias, I. Yusoff, Removal of Cd(II) onto *Raphanus sativus* peels biomass: equilibrium, kinetics, and thermodynamics, *Desal. Water Treat.*, 51 (2013) 22–24.
- [36] C.H. Giles, T.H. Mac Ewan, S.N. Nakhwa, D. Smith, Studies in adsorption. Part XI. A system of classification of solution adsorption isotherms and its use in diagnosis of adsorption mechanisms and in measurement of specific surface areas of solids, *J. Chem. Soc.*, 4 (1960) 3973–3993.
- [37] S. Wang, Y. Boyjoo, A. Choueib, A comparative study of dye removal using fly ash treated by different methods, *Chemosphere*, 60(10) (2005) 1401–1407.
- [38] U.K. Garg, M.P. Kaur, V.K. Grag, D. Sud, Removal of hexavalent chromium from aqueous solution by agricultural waste biomass, *J. Hazard. Mater.*, 140 (2007) 60–68.
- [39] B. Onida, B. Bonelli, L. Flora, C.O. Arean, E. Garrone, Permeability of micelles in surfactant-containing MCM-41 silica as monitored by embedded dye molecules, *Chem. Commun.*, 21 (2001) 2216–2217.
- [40] Z. Yermiyahu, I. Lapidés, S. Yariv, Visible absorption spectroscopy study of the adsorption of Congo Red by montmorillonite, *Clay Miner.*, 38 (2003) 483–500.
- [41] L. Wang, A. Wang, Adsorption properties of Congo Red from aqueous solution onto surfactant-modified montmorillonite, *J. Hazard. Mater.*, 160 (2008) 173–180.
- [42] M.A. Ashraf, M. Hussain, K. Mahmood, A. Wajid, M. Yusof, Y. Alias, I. Yusoff, Removal of acid yellow-17 dye from aqueous solution using eco-friendly biosorbent, *Desal. Water Treat.*, 51 (2013) 4530–4545.
- [43] V. Vimonses, S. Lei, B. Jin, C.W. Chow, C. Saint, Kinetic study and equilibrium isotherm analysis of congo red adsorption by clay materials, *Chem. Eng. J.*, 148(2–3) (2009) 354–364.
- [44] S. Chatterjee, D.S. Lee, M.W. Lee, S.H. Woo, Adsorption of congo red by chitosan hydrogel beads impregnated with carbon nanotubes, *Bioresour. Technol.*, 100 (2009) 3862–3868.
- [45] I. Langmuir, The adsorption of gases on plane surfaces of glass mica and platinum, *Am Chem Soc.*, 40 (1918) 1361–1403.
- [46] H.M.F. Freundlich, Über Die Adsorption in Lösungen, *Zeitschrift für Physikalische Chemie.*, 57 (1906) 385–470.
- [47] G. Rytwo, E. Ruiz-Hitzky, Enthalpies of adsorption of methylene blue and crystal violet to montmorillonite, *J. Therm. Anal. Calorim.*, 71(3) (2003) 751–759.
- [48] A. Demirbas, A. Sari, O. Isildak, Adsorption thermodynamics of stearic acid onto bentonite, *J. Hazard. Mater.*, 135(1) (2006) 226–231.
- [49] R. Gong, Y. Sun, J. Chen, H. Liu, C. Yang, Effect of chemical modification on dye adsorption capacity of peanut hull, *Dyes Pig.*, 67 (2005) 175–181.
- [50] I. Javed, F. Mateen, U. Rafique, N. Tabassum, K.S. Balkhair, M.A. Ashraf, Synthesis of zeolite from marble powder waste: a greener approach and its application for the removal of inorganic metals from wastewater, *Desal. Water Treat.*, 57(22) (2016) 10422–10431.